

FAILSAFE: HIGH-PERFORMANCE RESILIENT SERVING

Ziyi Xu¹ Zhiqiang Xie² Swapnil Gandhi² Christos Kozyrakis^{2,3}

ABSTRACT

Tensor parallelism (TP) enables large language models (LLMs) to scale inference efficiently across multiple GPUs, but its tight coupling makes systems fragile: a single GPU failure can halt execution, trigger costly KVCache recomputation, and introduce long-term compute and memory imbalance. We present FailSafe, a fault-tolerant TP serving system that sustains high performance under irregular GPU availability. FailSafe introduces three techniques to balance computation and memory across GPUs: (1) Cyclic KVCache Placement for even memory utilization, (2) Hybrid Attention combining tensor- and data-parallel attention to eliminate stragglers, and (3) Fine-Grained Load-Aware Routing to dynamically balance requests. It further employs proactive KVCache backup and on-demand weight recovery to avoid expensive recomputation and redundant data transfers.

We implement these techniques in a lightweight serving engine compatible with existing LLM infrastructures. Evaluated on an 8×H100 DGX system with real-world fault traces and representative workloads, FailSafe achieves up to 2× higher throughput and two orders of magnitude lower recovery latency compared to standard fault-handling approaches. Even with up to three GPU failures, FailSafe sustains high throughput and balanced utilization, demonstrating robust and efficient LLM serving under dynamic and unreliable hardware conditions.

1 INTRODUCTION

Modern Large Language Models (LLMs) have significantly advanced capabilities across diverse applications, including conversational agents (OpenAI, 2022), search engines (Gemini), code generation (Github, 2024), and scientific discovery. As these models scale rapidly—now comprising hundreds of billions or even trillions of parameters—their computational and memory requirements have risen dramatically (DeepSeek-AI, 2024). Consequently, deploying LLM inference workloads increasingly demands aggregation of compute and memory resources across multiple GPUs, often distributed over several nodes. Tensor parallelism (TP) has emerged as a prominent solution for efficiently scaling these workloads by tightly coupling GPUs¹ using high-bandwidth interconnects such as NVIDIA’s NVLink (NVIDIA), AMD’s infinity fabric link (AMD) or Google’s TPU Pods (Google).

While TP enables efficient scaling within a *scale-up domain*—a set of GPUs connected via high-bandwidth interconnects—it also inherently couples all participating devices (Shoeybi et al., 2019). This tight coupling creates a double-edged sword: a single GPU failure can render

the entire TP execution unavailable across all GPUs within the affected scale-up domain. With scale-up domain sizes steadily increasing—with current deployments reaching up to 72 GPUs (NVIDIA, 2025a)—the probability and impact of GPU failures both intensify. Recent studies (He et al., 2023; Hu et al., 2024; Kokolis et al., 2025; Jiang et al., 2024) underline the rising frequency of GPU failures, attributing them to hardware degradation, thermal instability, and unpredictable preemptions. These failures impose substantial hurdles for maintaining reliable, high-performance inference services, critically affecting user experience and overall system efficiency. Typically, GPU failures introduce two primary types of overhead:

Challenge #1: Recovery Overhead. When a GPU fails, several immediate complications arise in reassigning inference workloads. First, the KVCache for all inflight requests previously managed by the failed GPU is irrecoverably lost, requiring expensive and time-consuming recomputation before inference can continue. Additionally, the surviving GPUs must reshuffle and rebalance model weights (stored in CPU DRAM or persistent storage), resulting in substantial data movement and traffic over PCIe. Collectively, these recovery tasks—KVCache reconstruction and model weight reshuffling—trigger significant latency spikes, stall in-flight requests, and severely degrade the quality of experience for clients, as depicted in Figure 12.

Challenge #2: Persistent Imbalance Overhead. After recov-

Under Review ¹Shanghai Jiao Tong University ²Stanford University ³NVIDIA Research. Correspondence to: Ziyi Xu <xzy2022@sjtu.edu.cn>, Christos Kozyrakis <kozyraki@stanford.edu>.

¹We use “GPU” to refer to AI accelerators generally, such as GPUs, TPUs, and Trainium

ery, the system continues with fewer GPUs than originally provisioned (e.g., from 8 to 7), breaking the symmetry assumptions under which serving pipelines are tuned. The result is enduring compute and memory skew. Compute imbalance occurs primarily due to uneven workload distribution, notably within attention layers partitioned by discrete attention heads. This imbalance leads to some GPUs idling, awaiting heavily loaded GPUs to complete their tasks, resulting in stalled resources and significantly diminished throughput. Concurrently, memory imbalance arises from unequal distribution of KVCache utilization across GPUs. This memory imbalance limits available cache capacity, forcing smaller batch sizes and further constraining throughput due to increased overhead from frequent kernel launches and reduced parallelism. These persistent imbalances, depicted in Figures 1 and 2, consistently impose performance bottlenecks and cause severe underutilization of valuable GPU resources.

To address these challenges, we propose FailSafe, a system designed to provide high-performance yet resilient TP serving under irregular GPU availability. FailSafe introduces three key techniques to sustain efficiency and balance under irregular GPU availability: (1) *Cyclic KVCache Placement*, which rotates KVCache placement across layers to evenly distribute memory usage and preserve effective batch size; (2) *Hybrid Attention*, which integrates TP- and DP-style attention to balance computation across GPUs and eliminate stragglers; and (3) *Fine-Grained Load-Aware Routing*, which dynamically dispatches requests based on real-time GPU load to reduce intra-batch workload imbalance.

In addition, FailSafe incorporates proactive KVCache backup to eliminate time-consuming recomputation during recovery, and on-demand weight restoration to minimize I/O overhead. During normal operation, KVCache backups are asynchronously maintained in the background. Upon failure, each GPU restores only the necessary subset of lost KVCache and model weights in a joint, non-redundant manner, thereby avoiding excessive PCIe data transfers and accelerating recovery.

We implement these mechanisms in a lightweight serving engine that integrates seamlessly with existing LLM infrastructures. Evaluated on an $8 \times$ H100 DGX system using real-world fault traces and representative serving workloads, FailSafe demonstrates strong performance across both offline throughput-optimized and online latency-constrained scenarios. It achieves up to $2 \times$ higher throughput and up to two orders of magnitude lower recovery latency compared to standard fault-handling practices. Further analysis shows that FailSafe continues to deliver substantial performance benefits even when up to three of eight GPUs fail, highlighting its robustness and scalability under severe fault conditions.

2 RESILIENT MODEL SERVING

2.1 Background

2.1.1 LLM Inference

Most popular LLMs are based on the Transformer architecture, comprising multiple stacked transformer layers (Vaswani et al., 2017). Each layer consists of an attention mechanism and a feed-forward network (FFN). Attention layers enable tokens within a request to interact, while FFN layers process tokens independently. Most LLMs adopt the auto-regressive decoding mechanism, leading to an incremental inference process consisting of several iterations (Yu et al., 2022). At each inference iteration, the model predicts the next token based on all previously generated tokens. To optimize performance and avoid redundant computation, LLM serving systems cache intermediate token states—known as the KVCache—for reuse in subsequent token generation steps (Zheng et al., 2025; Kwon et al., 2023). This caching strategy divides the inference process into two distinct phases: the prefill phase, which processes all input tokens simultaneously in a single iteration to construct the initial key-value cache and generate the first output token; and the decoding phase, where only the newly generated token requires computation to update the KVCache.

2.1.2 Multi-GPU LLM Inference

Modern LLMs frequently exceed the memory capacity and performance capabilities of single GPUs, necessitating distributed execution strategies. Inference parallelism differs fundamentally from training parallelism, as it involves only forward-pass computations—without gradients—and introduces specific challenges such as efficient management of the key-value (KV) cache. Effective parallelism schemes typically aim either to minimize latency for individual inference requests or to maximize the overall throughput of concurrent workloads. Common parallelism strategies include data parallelism (DP), where the model is replicated across multiple nodes to independently handle separate requests, and pipeline parallelism (PP), where model layers are distributed sequentially across nodes to balance computational load and memory usage. Among these methods, tensor parallelism (TP)—which partitions model parameters and KVCache evenly across all GPUs within a node—stands out. TP uniquely leverages high-bandwidth interconnects within a node to reduce inference latency by splitting large matrix operations across GPUs. Hybrid Parallelism combines TP and PP, often using TP within compute nodes and PP across nodes, to scale to larger models and GPU counts.

2.1.3 Frequent Failures in Large-Scale Clusters

Modern inference-serving clusters routinely consist of thousands of GPUs interconnected by sophisticated networking,

storage, and power infrastructures. At this scale, hard failures—complete, sudden, and persistent hardware disruptions—occur frequently and inevitably. Common sources of these hard failures include GPU overheating, ECC errors, CUDA errors, and GPU driver errors leading to abrupt termination of system software running on them (Hu et al., 2024). For instance, Alibaba Cloud (He et al., 2023) reported abnormal termination rates as high as 44% for its top 5% most resource-intensive workloads. Similar reliability challenges have been echoed by Meta (Kokolis et al., 2025), ByteDance (Jiang et al., 2024), LAION (Beaumont, 2022), and Google (Zu et al., 2024).

2.2 Motivation and Challenges

2.2.1 Imbalanced Load over Irregular Hardware Configurations

When deploying LLMs on an irregular number of GPUs, for example, seven instead of the ideal eight due to GPU availability issues discussed in §2.1.3, it becomes challenging to maintain balanced computation and memory usage across devices. For feed-forward (FFN) layers, weights are typically partitioned along the intermediate dimension, allowing relatively even distribution even across fewer GPUs, since the intermediate dimension is large enough to divide smoothly. In contrast, attention layers are divided by attention heads, which are usually limited to only tens per layer, leading to severe imbalance when sharded across an irregular number of GPUs.

For instance, when sharding a LLaMA-3.1-70B model (Meta-AI, 2024) with 8 key-value heads across seven GPUs, some ranks inevitably host two heads while others hold only one, resulting in up to a $2\times$ slowdown in attention-layer computation (Figure 2). This imbalance is further exacerbated in long-context scenarios, where each attention head contributes not only to computation but also to the KVCache memory footprint. As a result, certain ranks may consume up to twice as much KVCache memory as others. Due to the synchronized nature of tensor parallelism, such imbalance effectively reduces the usable batch size of the entire system, leading to substantial throughput degradation, as shown in Figure 1.

2.2.2 Latency Spike due to State Loss

When a GPU suddenly fails or becomes temporarily unavailable, all model parameters and KVCache residing on it are immediately lost. While static model weights can be reloaded from persistent storage such as host memory or disk with moderate cost, the KVCache represents the dynamic per-request state that must be recomputed from scratch. This recomputation requires rerunning the entire prefill phase for all affected in-flight requests, which is an extremely compute-intensive process. In our online serving

experiments (Section 4.3.3), recomputing the lost KVCache alone takes over 20 seconds, during which all affected requests undergo severe stalls. Moreover, this backlog propagates through the serving pipeline, introducing queuing delays that further impact subsequent requests. The result is a sharp latency spike and widespread SLO violations, significantly degrading user-perceived quality of service. This phenomenon highlights the urgent need for fast recovery mechanisms. Instead of recomputing from scratch, a more effective strategy is needed to speed up this entire recovery process.

3 DESIGN AND IMPLEMENTATION

To enable model execution on an irregular number of GPUs, we first implement a vanilla form of *non-uniform tensor parallelism* for model serving, originally proposed in prior work on fault-tolerant LLM training (Arfeen et al., 2025). Non-uniform tensor parallelism allows model weights and computations to be distributed unevenly across GPUs by adjusting synchronization among tensor-parallel workers. This enables flexible tensor-parallel configurations under partial GPU availability. To address the load imbalance and latency spikes discussed in §2.2, we further introduce a memory and computation balancer and a lighting recovery mechanism for higher throughput and better SLO attainment.

3.1 Memory and Computation Balancer

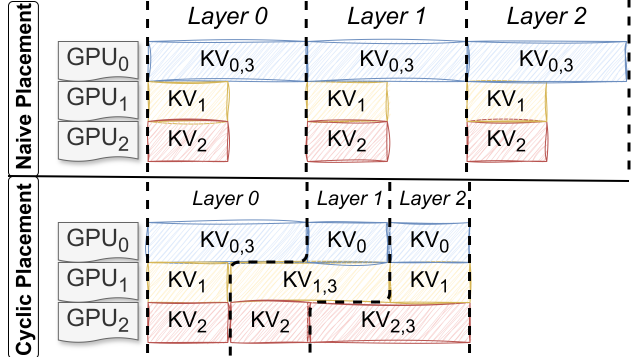


Figure 1. Illustration of the proposed cyclic placement for balancing KVCache memory usage across GPUs. In this example, the model has 4 key-value heads and deploys non-uniform TP3. KV_i stands for the KVCache for *i*-th key value head. Cyclic placement (bottom) improves overall KVCache capacity by approximately 50%, compared with a naïve placement (top).

Cyclic Placement. To mitigate memory imbalance, we propose a simple yet effective cyclic placement strategy. Specifically, attention heads and their corresponding KVCache blocks are distributed cyclically across GPUs. As illustrated in Figure 1, naïve placement can lead to signif-

icant KVCache skew, where some GPUs accumulate substantially larger memory footprints. In contrast, our cyclic scheme rotates attention-head assignments layer by layer, ensuring that across every contiguous n layers in a TP_n configuration, the aggregate KVCache allocation remains well balanced. Because modern LLMs typically contain tens or even hundreds of layers—far exceeding the usual tensor-parallel world size (often below ten)—this cyclic distribution effectively smooths out KVCache memory utilization across all GPUs.

However, this strategy alone does not fully resolve computational imbalance. Each attention layer still performs an all-reduce operation before and after attention computation, synchronizing results across all GPUs. Thus, while cyclic placement balances memory consumption across layers, within each layer some GPUs continue to perform more computation than others, leading to temporary stalls.

Hybrid Attention. To further mitigate intra-layer computation imbalance, we introduce Hybrid Attention, which maintains a balanced workload among tensor-parallel workers by assigning each the same number of attention heads and leveraging data parallelism (DP) to handle the remaining heads. Hybrid Attention can be viewed as a generalization of TP and DP.

For example, in the LLaMA-3 70B model with eight attention heads, a deployment with eight TP workers evenly distributes the heads, behaving identically to a standard TP_8 configuration. However, when only seven GPUs—and hence seven TP workers—are available, each TP worker receives one head, while the remaining head is replicated across all seven GPUs. Each GPU thus also acts as a DP worker, processing the replicated head for different requests. This design enables the computation of the extra head to be parallelized across GPUs through data parallelism, distributing requests to balance the workload effectively. As shown in Figure 2, naïve non-uniform tensor parallelism often results in straggler GPUs during attention computation, causing under-utilization. In contrast, Hybrid Attention distributes the computation of replicated heads for different requests across multiple GPUs, significantly reducing intra-layer imbalance, minimizing idle time, and improving overall utilization.

Notably, the widely adopted DP attention design (SGLang-Team, 2024)—used for serving multi-head latent attention (MLA) (DeepSeek-AI et al., 2024) models such as DeepSeek-V3 (DeepSeek-AI, 2024)—is a special case of our Hybrid Attention. While DP attention duplicates a single attention head across all GPUs, Hybrid Attention generalizes this approach to flexibly support both partitioned (TP) and replicated (DP) heads within the same layer.

However, DP alone does not guarantee perfect balance, since

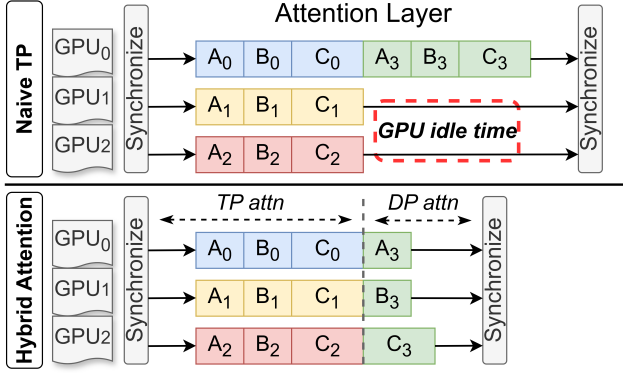


Figure 2. Illustration of the proposed hybrid attention. In this example, the model has 4 key-value heads and deploys non-uniform TP_3 . A_i stands for the i -th head’s computation for request A . Request A is routed to GPU₀, B to GPU₁, and C to GPU₂. Hybrid attention (bottom) combine TP attention with DP attention, significantly reducing GPU idle time and improving GPU utilization.

input requests can be inherently skewed. Even if all DP replicas process the same number of requests, some GPUs may experience longer execution times due to variable input lengths. In highly skewed workloads—especially in long-context scenarios—the system may temporarily revert to behavior similar to naïve non-uniform TP, where faster GPUs must still wait for the longest-running task.

Fine-grained Load-aware Router. To further mitigate the load imbalance caused by skewed input request distributions, we introduce a fine-grained, load-aware routing mechanism that dynamically balances the workload among DP workers across GPUs. Our scheduler design addresses two complementary aspects: (1) *routing DP ranks*, and (2) *forming compute-balanced batches*.

Load-Aware DP-Rank Routing. We observe that the DP-rank scheduling problem can be modeled as an instance of the classical *online makespan minimization* problem (Dwibedy & Mohanty, 2022; 2020; Wang et al., 2025). To achieve low scheduling overhead while maintaining balance, we adopt a simple yet effective greedy strategy: each incoming request is assigned to the GPU with the smallest estimated remaining workload. Here, the workload is defined as the total pending DP computation (in token units) currently queued on each GPU. This dynamic routing policy continuously adapts to runtime variations in request arrival patterns, preventing load concentration on specific GPUs.

Fine-Grained Chunked Prefill. To complement routing, we design a *Fine-Grained Chunked Prefill* mechanism for the prefill stage. Unlike conventional chunked prefill, which allows only one chunk per request in a batch. Our approach permits chunks from multiple requests to be executed jointly

Algorithm 1 DP-aware Adaptive Chunked Prefill

Input: Token budget N , rank set \mathcal{R} , schedulable tokens $\{S_r\}$, workloads $\{W_r\}$

Output: Next Prefill batch B

```

 $L_r \leftarrow 0$  {initialize load per rank}
 $B \leftarrow \emptyset$  {initialize current prefill batch}
 $H \leftarrow \emptyset$  {initialize candidate batch set}
while  $|B| < N$  and  $\exists r : S_r \neq \emptyset$  do
   $r^* \leftarrow \arg \min_{r \in \mathcal{R}, S_r \neq \emptyset} L_r$  {least-loaded rank}
   $t \leftarrow \text{first}(S_{r^*})$ ,  $S_{r^*} \leftarrow S_{r^*} \setminus \{t\}$  {schedule 1 token}
   $B \leftarrow B \cup \{t\}$ ,  $L_{r^*} \leftarrow L_{r^*} + \text{cost}(t)$ ,  $H \leftarrow H \cup \{B\}$ 
end while
return choose_best_batch( $H$ )

```

within the same batch. Since the computational cost of prefill attention grows quadratically with sequence length, the cost of processing a chunk of size N after L processed tokens is $\mathcal{O}(N^2 + NL + N)$. To maintain balanced GPU workloads and prevent out-of-memory errors, we define a global prefill token budget N representing the maximum number of tokens per batch. Tokens are then iteratively allocated to the least-loaded GPU until the budget is reached, ensuring balanced computation and bounded intermediate memory usage. Algorithm 1 outlines the adaptive chunked prefill procedure.

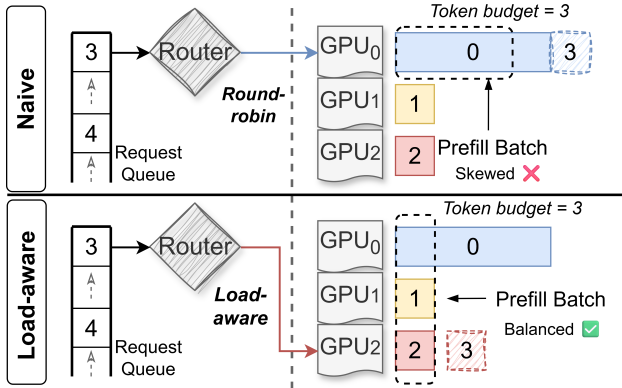


Figure 3. Illustration of the load-aware router and scheduler. In this example, request 0 has 4 tokens, request 1 and 2 has 1 token, and a new request 3 with 1 token arrives. In the naïve setting (top), a round-robin router combined with a FIFO chunked prefill scheduler results in an highly unbalanced prefill batch: within the prefill token budget (which is 3), only a chunk of request 0 is scheduled in the prefill batch. In contrast, our load-aware router (bottom) dynamically redirects new requests to the least-loaded GPU, and our adaptive chunked prefill mechanism helps form a balanced batch.

As shown in Figure 3, naïve routing and chunked prefill lead to highly skewed batches and unbalanced GPU workloads. In the example, GPU₀ becomes overloaded because the

vanilla scheduler includes only the first chunk of request 0 within the prefill budget, leaving other GPUs underutilized. In contrast, our load-aware router dynamically assigns DP ranks based on real-time GPU load, while the adaptive chunked prefill scheduler constructs balanced batches in a best-effort manner. Together, these two mechanisms significantly improve GPU utilization and overall system throughput under dynamic and skewed request patterns.

3.2 Lightning Recovery

As discussed in §2.2.2, rapid recovery is critical to prevent request backlogs and maintain SLO compliance. We identify two dominant sources of recovery latency: recomputation of the lost KVCache and reloading of re-sharded model weights. To mitigate both, we propose a *Lightning Recovery* framework comprising two components—*Proactive KVCache Backup* and *On-Demand Weight Recovery*—that together minimize downtime by avoiding redundant recomputation and restoring only essential model data.

Proactive KVCache Backup. When a GPU fails, its associated KVCache is lost, requiring a costly re-prefill phase to regenerate it. To enable fast recovery, FailSafe proactively backs up KVCache data to host memory. Modern GPU servers typically equip ample and persistent CPU memory that are larger than the GPU HBMs, which remains intact even after GPU faults, making it ideal for lightweight state preservation. Restoring KVCache from host memory is often substantially faster than recomputing it as long as PCIe bandwidth is well utilized (Xie et al., 2025), offering both practicality and efficiency.

Upon failure, surviving GPUs reuse their existing KVCache, while each GPU reloads only its required portion from host memory. Thanks to the cyclic KV placement optimization discussed in §3.1, the reloaded cache is evenly distributed across GPUs, balancing PCIe transfer bandwidth during recovery.

On-demand Weight Recovery. Reusing and restoring the KVCache eliminates recomputation overhead, but model weight reloading can still be a bottleneck. To address this, FailSafe leverages a key mathematical property: the sharding order of FFN weights can be freely permuted without affecting correctness, as matrix multiplication is commutative along the reduction dimension.

In conventional tensor-parallel inference, FFN weights are sharded contiguously along the intermediate dimension, so when the TP world size changes (e.g., from 8 to 7 due to a GPU fault), existing shards misalign with new ranks, forcing full-shard reloads. By exploiting the commutativity of matrix multiplication, FailSafe allows each rank to reload only the required subset of weights instead of an entire shard, significantly reducing data transfer and recovery time.

For attention layers, FailSafe employs DP-based placement within its hybrid attention design. To minimize redundant PCIe transfers, each rank loads a distinct portion of the DP weights from host memory and exchanges missing segments with peers via NVLink. Because NVLink offers far higher bandwidth than PCIe, the synchronization overhead is minimal and can be overlapped with ongoing weight loading. Together, these two strategies ensure that all ranks participate equally in recovery, fully utilizing NVLink and PCIe bandwidth while minimizing end-to-end recovery latency.

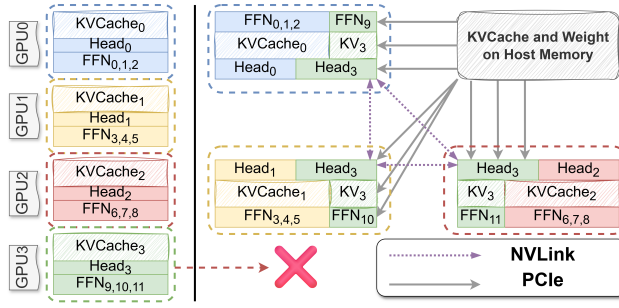


Figure 4. On-demand Recovery mechanism. In this example, the FFN weights are divided into 12 shards and there’re 4 attention heads with corresponding KVCache. The system starts with normal TP4. When GPU 3 fails, we will restore all the lost state (weights and KVCache) via PCIe. Our On-demand recovery mechanism eliminate all redundant PCIe transfer.

Figure 4 illustrates the on-demand recovery process under a TP4 setup. The model has 12 FFN shards, 4 attention heads, and 4 KVCache partitions distributed across three GPUs. When GPU3 fails, a naïve TP3 fallback would force GPU3 to load the entire missing shards (FFN_{9,10,11}) and attention head₃. In contrast, FailSafe enables each surviving GPU to reload only a fraction of the missing weights by leveraging FFN commutativity. For the lost attention head, hybrid attention divides the required weights across GPUs, synchronizing the remaining segments via high-bandwidth NVLink. Meanwhile, each rank recovers only the necessary subset of the missing KVCache from host memory, completing recovery quickly and in parallel.

4 EVALUATION

We evaluate FailSafe on a server equipped with eight NVIDIA H100 GPUs (80 GB each). The GPUs are interconnected via 4th-generation NVLink and each GPU is connected to the CPU via a PCIe 5.0 x16 link. We measure both system offline throughput as well online throughput latency characterization to demonstrate the overall effectiveness of our system. To ensure a comprehensive evaluation, we experiment with two representative large language models that normally utilize a whole node of GPUs to serve: a dense

model, LLaMA-3.1-70B-Instruct (Meta-AI, 2024), and a mixture-of-experts (MoE) model, Mixtral-8x22B-Instruct v0.1 (Mistral-AI, 2024). We implemented FailSafe on top of a light-weight customized LLM serving engine, which is implemented using around 7k lines of code and achieves performance on par with state-of-the-art open-source LLM inference frameworks such as vLLM (Kwon et al., 2023) and SGLang (Zheng et al., 2025).

4.1 Offline Throughput under Faulty Environments

Failure Simulation. We simulate failure and recovery events on an 8×8 H100 cluster using a real-world failure trace derived from the GCP cloud availability dataset, which has been widely adopted in prior studies such as Bamboo (Thorpe et al., 2023), Ooblock (Jang et al., 2023), and Recycle (Gandhi et al., 2024). The trace is scaled such that full availability corresponds to 64 GPUs, as illustrated in Figure 5. During the simulation, each failure event randomly disables one GPU across the eight nodes, while each recovery event randomly restores one of the failed GPUs. Upon every GPU failure, the system must reconfigure itself to continue operation with the reduced number of GPUs. For simplicity, we fix the reconfiguration (switching) latency to 10 seconds for all systems, as this delay has negligible impact on the overall throughput.

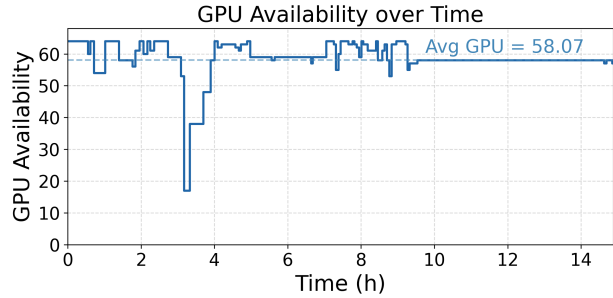


Figure 5. GPU availability from GCP cloud availability traces.

Workload Dataset.

We use *OpenThoughts-114k* (Guha et al., 2025), a large-scale, high-quality “thinking” dataset composed of 114,000 multi-turn reasoning and instruction-following examples curated from diverse sources. This dataset is widely used for evaluating and post-training LLMs on reflective and logical reasoning tasks, making it representative of realistic LLM-serving workloads. Its key input–output characteristics are summarized in Table 1. We adopt this dataset to emulate long-context, multi-turn interactions that commonly arise in RL-based training and inference workloads (Ouyang et al., 2022).

Baselines. We compare FailSafe against three configura-

Available GPUs	1	2	3	4	5	6	7	8
Baseline System	—	—	—	4	4	4	4	8
FailSafe	—	—	3	4	5	6	7	8

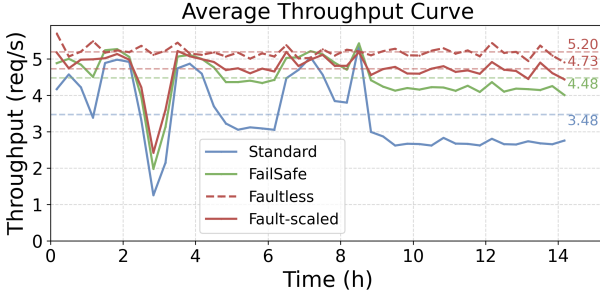


Figure 6. (a) LLaMA-3.1-70B-Instruct

Available GPUs	1	2	3	4	5	6	7	8
Baseline System	—	—	—	—	—	—	—	8
FailSafe	—	—	—	—	5	6	7	8

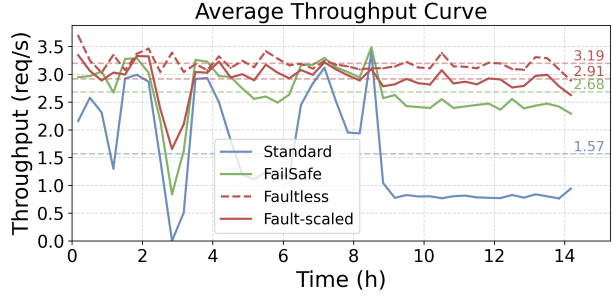


Figure 7. (b) Mixtral-8x22B-Instruct-v0.1

Figure 8. The tables above summarize the tensor-parallel configurations adopted by each system under different numbers of available GPUs per node. The figures below show the corresponding real-time throughput of different systems during fault-injection experiments. Dashed lines in each figure represent the average throughput over time.

Metric	Mean	Median	Max
Input length (tokens)	422	352	7633
Output length (tokens)	7295	5583	37817

Table 1. Input-output characteristics of OpenThought dataset.

tions: (1) a non-fault-tolerant *baseline* system, (2) a *fault-free* system that assumes no GPU failures and serves as the performance upper bound, and (3) a *fault-scale* system that linearly scales the throughput of the *fault-free* case based on GPU availability. We use a single 8-GPU machine to emulate eight independent 8-GPU nodes and report aggregated throughput across all simulated nodes. All systems employ tensor parallelism within each node. In the *baseline* system, the per-node TP configurations are limited to 1, 2, 4, 8 GPUs, consistent with the implementations of state-of-the-art serving engines such as SGLang and vLLM. Consequently, when a GPU fails within a node, the *baseline* system must fall back to the next supported configuration, resulting in reduced resource utilization. In contrast, FailSafe supports flexible TP configurations with arbitrary GPU counts, provided sufficient memory is available for model weights and KVCache. The same flexibility applies to the *fault-scale* setting. As shown in Figure 8, the minimum number of GPUs required to serve the dense LLaMA-3.1-70B-Instruct model is three. For the Mixture-of-Experts model Mixtral-8x22B-Instruct-v0.1, the larger memory footprint raises this minimum to five GPUs.

Performance Analysis. As shown in Figure 8, FailSafe consistently outperforms the standard TP4 baseline across both dense and MoE models. For *LLaMA-3.1-70B*, FailSafe de-

livers 1.28 \times higher average throughput, achieving 95% of the *Fault-scaled* performance, demonstrating the effectiveness of its memory and compute balancing optimization. For *Mixtral-8x22B*, the throughput gain increases to 1.71 \times , reaching 92% of the *Fault-scaled* performance. The larger throughput improvement stems from Mixtral’s higher memory footprint, where the standard TP4 configuration becomes infeasible, leading to greater resource underutilization that FailSafe effectively mitigates.

4.2 Throughput-Latency of Fault-tolerant Online Serving

We further evaluate the throughput-latency characteristics of FailSafe under online serving scenarios. To ensure consistency, we measure throughput and latency by varying the input request rate in stable environments, i.e., the system operates with a fixed number of available GPUs and no runtime reconfiguration. We separately analyze the *prefill* and *decode* stages, as prefill-decode (P-D) disaggregation (Zhong et al., 2024) is a standard practice in modern LLM serving for improved latency SLO attainment (NVIDIA, 2025b). Latency is reported using *Time to First Token* (*TTFT*) for prefill instances and *Time Between Tokens* (*TBT*) for decode instances. Throughput is measured as input-token throughput for prefill and generated-token throughput for decode.

Dataset. We use the real-world Mooncake (Qin et al., 2025) conversation trace, a popular open-source trace with arrival timestamps of requests as well as anonymized input and output sequence lengths. We randomly sampled 3,000 requests out of the complete traces and scale the timestamp for scanning different request rates. Table 2 summarizes the input and output characteristics of the selected trace.

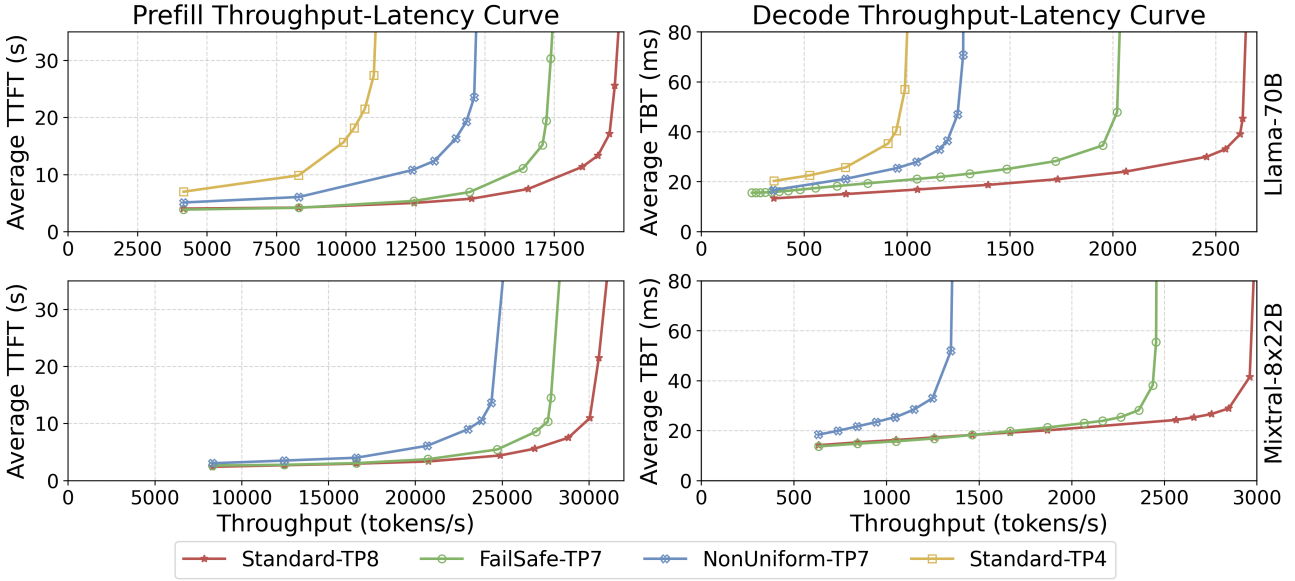


Figure 9. Throughput-latency curves when serving the Mooncake trace. The TP4 baseline is omitted for the Mixtral-8x22B model due to insufficient memory to accommodate both model weights and KVCache on only 4 GPUs.

Requests are issued according to the scaled timestamps, and we record TTFT, TBT, and token throughput for each system. By varying the scaling ratio, we obtain the complete throughput-latency curves.

Baselines. We compare FailSafe against three baselines: (1) *Standard-TP4*, the default fallback tensor-parallel configuration activated upon GPU failure, serving as the primary baseline; (2) *Standard-TP8*, the fault-free configuration representing the upper-bound performance; and (3) *Nonuniform-TP7*, a naïve implementation that operates on seven GPUs but suffers from significant load imbalance. Our proposed FailSafe adopts the optimized *FailSafe-TP7* configuration, which integrates all key components—cyclic memory placement, hybrid attention, and a load-aware router and scheduler. We focus on the 7-GPU setting as it represents the most common failure scenario in practice; additional experiments under higher failure rates are presented in §4.3.1. Note that the *Standard-TP4* baseline is omitted for the Mixtral-8x22B experiment, as the model weights and KVCache for the longest requests cannot fit within the memory capacity of only four GPUs.

Performance Analysis. Figure 9 presents the through-

put-latency characteristics of FailSafe compared with all baselines across both the prefill and decode stages. For both the dense *LLaMA-3.1-70B* and the MoE *Mixtral-8x22B* models, FailSafe consistently outperforms *Standard-TP4* and *Nonuniform-TP7* under all request rates. At low request rates, it achieves near-optimal performance comparable to the fault-free *Standard-TP8* configuration.

In the prefill stage, FailSafe attains up to 2× and 1.28× higher throughput than *Standard-TP4* and *Nonuniform-TP7*, respectively, under the same 10s TTFT constraint for *LLaMA-3.1-70B*, and achieves a 1.14× gain over *Nonuniform-TP7* for *Mixtral-8x22B*.

In the decode stage, where balanced memory and compute utilization becomes more critical, the benefits are even more pronounced. Under a 40ms TBT constraint, FailSafe achieves up to 2× and 1.60× higher throughput than *Standard-TP4* and *Nonuniform-TP7* for *LLaMA-3.1-70B*, and a 1.85× improvement over *Nonuniform-TP7* for *Mixtral-8x22B*.

4.3 Performance Breakdown Analysis

4.3.1 Hybrid Attention with Less GPUs

To further evaluate the effectiveness of our Hybrid Attention mechanism, we measure system throughput across different TP configurations. We compare FailSafe against the *Nonuniform-TP* baseline under TP5–TP7 settings and report the peak throughput on the Mooncake trace using the *LLaMA-3.1-70B* model.

As shown in Figure 10, when running with four or eight

Metric	Mean	Median	Max
Input length (tokens)	13,516	8,001	12,3192
Output length (tokens)	349	362	2,000
Total requests			3,000

Table 2. Input-output characteristics of our scaled Mooncake trace.

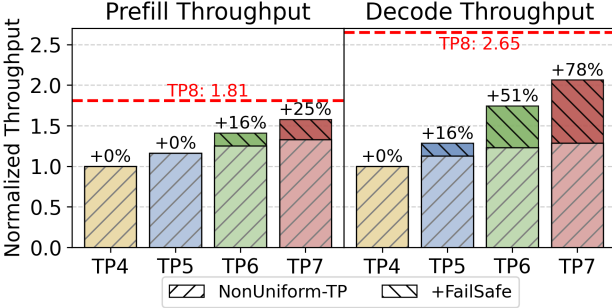


Figure 10. Performance comparison of FailSafe optimization with Nonuniform-TP. Throughput is normalized to Standard-TP4.

GPUs (TP4/TP8), both systems degenerate to standard uniform tensor parallelism and therefore exhibit identical performance. As the tensor-parallel world size becomes irregular (beyond four GPUs), computation and memory imbalance intensifies, and FailSafe begins to demonstrate clear advantages. In the prefill stage, FailSafe achieves performance gains of 0%, 16%, and 25% over Nonuniform-TP for TP5, TP6, and TP7 configurations, respectively. The limited improvement under TP5 arises because compute imbalance at this scale is inherently harder to mitigate. In contrast, during the memory-bound decode stage, the benefits become more pronounced—FailSafe improves throughput by 16%, 51%, and 78% for TP5, TP6, and TP7, respectively. These results demonstrate that the proposed hybrid attention design effectively alleviates intra-layer imbalance and scales efficiently under non-uniform GPU configurations.

4.3.2 Memory and Compute Balancing

Without memory balancing, certain GPUs store disproportionately larger portions of the KVCache and model weights, constraining the maximum batch size during the decode stage and leading to suboptimal GPU utilization. To quantify the impact of memory balancing, we first augment the baseline Nonuniform-TP7 configuration with cyclic memory placement, ensuring even distribution of KVCache and model weights across GPUs. To further highlight the effect of computation balancing introduced by our hybrid attention mechanism, we compare the peak throughput of four system configurations on the Mooncake trace using the *LLaMA-3.1-70B* model: (1) Standard-TP4 (baseline), (2) +Nonuniform-TP7, (3) +Memory-balancing (Nonuniform-TP7 with cyclic memory placement), and (4) +Compute-balancing, which integrates all proposed optimizations.

As shown in Figure 11, memory and compute balancing contribute differently across stages. In the prefill stage, the compute-balancing mechanism alleviates straggler effects and improves peak throughput by 25%, while memory balancing provides negligible benefit since prefill is primarily compute-bound. In contrast, the decode stage is

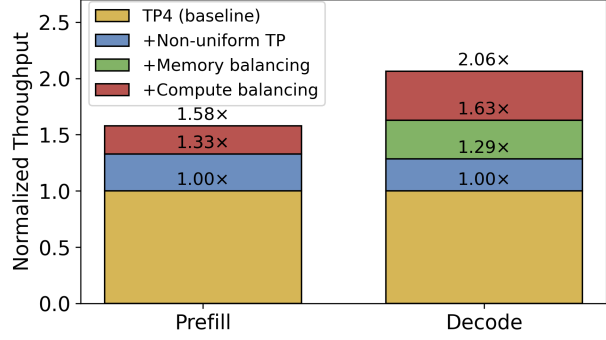


Figure 11. Breakdown of FailSafe optimization attributions in both prefill stage and decode stage on Llama-70B model.

memory-bound: larger batch sizes enabled by memory balancing significantly improve GPU utilization, yielding a 34% throughput increase. Finally, applying compute balancing on top of memory balancing further mitigates inter-GPU workload skew, boosting overall decode throughput by an additional 43%.

4.3.3 Recovery Latency

To evaluate the efficiency of our recovery mechanism, we conduct a detailed breakdown of recovery latency under online serving workloads, where latency sensitivity is most critical. We use the *LLaMA-3.1-70B* model and replay a contiguous 500-request window from the Mooncake conversation trace. The system initially runs with a standard TP8 decode instance, and a GPU failure is injected 100ms after the 250th request (i.e., halfway through the trace). We report the maximum *Time Between Tokens* (TBT) per request as the latency metric, since a request is considered to violate its decode SLO if any of its TBTs exceed the specified threshold.

All configurations enable memory and compute balancing optimizations. We compare the following recovery methods: (1) *Recompute*, which regenerates the lost KVCache and reloads all re-sharded model weights when transitioning to a TP7 configuration; (2) *FailSafe -Host*, which proactively backs up the KVCache in host memory and restores the lost cache from backup instead of recomputation; (3) *FailSafe -Full*, which builds upon *FailSafe -Host* and further avoids redundant PCIe transfers through joint on-demand weight loading; and (4) *FailSafe -Oracle*, which represents an idealized setting that restores only necessary metadata to the GPU without performing any weight or KVCache loading.

Table 3 summarizes GPU recovery latencies across settings. Compared to *Recompute*, restoring backed-up KVCache from host memory is 41.5× faster, while *FailSafe -Full* further reduces recovery latency by an additional 4.4×. These

Table 3. GPU state recovery latency of different systems.

System	Recompute	Host	Full	Oracle
Latency	22 s	530 ms	120 ms	15 ms
Speedup	1.00×	41.5×	183×	N/A

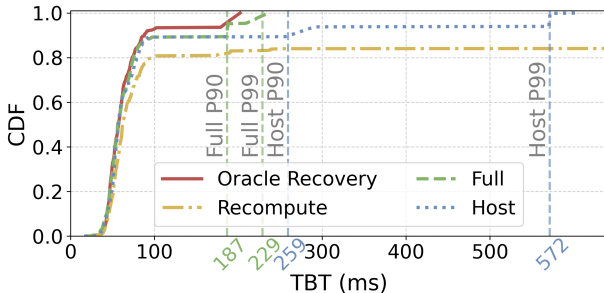


Figure 12. CDF of Max TBT per request of FailSafe under different recovery method. Dashed vertical lines shows the P90/P99 TBT of FailSafe Full and FailSafe Recompute.

improvements translate directly into user-perceived latency reductions. As shown in Figure 12, proactive host-side KVCache backup eliminates expensive recomputation, reducing P90 and P99 TBT from over 10s to under 1s. With on-demand weight loading, P99 TBT further drops from 572ms to 229ms, a $2.5\times$ improvement and approaching the oracle’s lower bound. Together, these results confirm that host-based KVCache backup and on-demand recovery are highly effective in minimizing recovery latency during online serving.

5 RELATED WORK

Fault tolerance in distributed training has been extensively studied by numerous systems. Redundancy-based methods such as Bamboo (Thorpe et al., 2023) incorporate redundant computations to handle preemptions common in cloud spot instances. Ooblock (Jang et al., 2023) employs heterogeneous pipelines to facilitate failure recovery without requiring additional spare resources, while ReCycle (Gandhi et al., 2024) dynamically reroutes computations to redundant data-parallel peers to seamlessly continue processing after failures. Checkpoint-based approaches include Check-Freq (Mohan et al., 2021), CPR (Maeng et al., 2021), and Gemini (Wang et al., 2023), which respectively mitigate checkpoint overhead by dynamically adjusting checkpoint frequency, quantizing embedding tables, and strategically scheduling checkpoint traffic across the storage hierarchy. Megascale (Jiang et al., 2024) addresses storage bottlenecks during recovery by efficiently sharing data between corresponding GPU workers across data-parallel groups. Unlike these training-focused systems, FailSafe specifically employs hybrid attention mechanism with non-uniform tensor

parallelism to achieve fault-tolerant distributed inference.

In the context of fault-tolerant distributed inference, recent efforts such as SpotServe (Miao et al., 2024), Llumnix (Sun et al., 2024), DejaVu (Strati et al., 2024), and Medusa (Zeng et al., 2025) enable live migration of KVCache and model weights. However, these systems do not address the persistent throughput degradation arising from compute and memory imbalances inherent in non-uniform tensor parallelism. To overcome these challenges, FailSafe integrates a hybrid attention mechanism and a dynamic scheduler alongside KVCache migration, ensuring both high-performance and robust resilience for distributed inference workloads.

6 DISCUSSION

Having demonstrated the advantages of FailSafe, we now discuss its applicability, limitations, and directions for future work. While tensor parallelism remains the dominant approach for scaling large models across multiple GPUs, it is not the only viable strategy. Other parallelism techniques offer inherent fault tolerance and may better suit specific model architectures. For instance, recent studies show that expert parallelism can achieve performance comparable to TP (SGLang-Team, 2025) for large MoE models, while exhibiting stronger resilience to partial GPU loss. Although our focus has been on fault-tolerant serving, FailSafe can also facilitate finer-grained resource sharing among concurrent jobs, mitigating starvation caused by rigid gang scheduling (Jeon et al., 2018). Integrating FailSafe with dynamic GPU resource allocation represents a promising direction for future exploration. As hardware platforms continue to scale, we expect FailSafe to become increasingly relevant for large multi-GPU systems such as NVL72 (NVIDIA, 2025a). While our evaluation focuses on single-node configurations, extending memory and compute balancing beyond NUMA boundaries remains an important avenue for future work.

7 CONCLUSION

We present FailSafe, a high-performance yet resilient serving system for tensor-parallel LLM inference under irregular GPU availability. FailSafe tackles the recovery overhead by introducing proactive KVCache backup and on-demand weight recovery, accelerating the recovery process by $183\times$ and thus avoiding a devastating latency spike in online serving. FailSafe also introduces cyclic KVCache placement, hybrid attention, and fine-grained load-aware router to eliminate the memory and computation imbalance between GPUs, achieving higher memory and computation utilization and up to $2\times$ higher throughput and two orders of magnitude faster recovery than standard fault-handling methods. Looking ahead, the principles behind FailSafe ex-

tend naturally to larger heterogeneous environments and to emerging architectures such as NVL72.

REFERENCES

AMD. Amd infinity fabric link. <https://www.amd.com/content/dam/amd/en/documents/instinct-tech-docs/other/56978.pdf>.

Arfeen, D., Mudigere, D., More, A., Gopireddy, B., Inci, A., and Ganger, G. R. Nonuniform-tensor-parallelism: Mitigating gpu failure impact for scaled-up llm training. *arXiv preprint arXiv:2504.06095*, 2025.

Beaumont, R. Large Scale OpenCLIP: L/14, H/14 and G/14 Trained on LAION-2B. <https://laion.ai/blog/large-openclip/>, 2022.

DeepSeek-AI. Deepseek-v3 technical report, 2024. URL <https://arxiv.org/abs/2412.19437>.

DeepSeek-AI, Liu, A., Feng, B., Wang, B., Wang, B., Liu, B., Zhao, C., Dengr, C., Ruan, C., Dai, D., Guo, D., Yang, D., Chen, D., Ji, D., Li, E., Lin, F., Luo, F., Hao, G., Chen, G., Li, G., Zhang, H., Xu, H., Yang, H., Zhang, H., Ding, H., Xin, H., Gao, H., Li, H., Qu, H., Cai, J. L., Liang, J., Guo, J., Ni, J., Li, J., Chen, J., Yuan, J., Qiu, J., Song, J., Dong, K., Gao, K., Guan, K., Wang, L., Zhang, L., Xu, L., Xia, L., Zhao, L., Zhang, L., Li, M., Wang, M., Zhang, M., Zhang, M., Tang, M., Li, M., Tian, N., Huang, P., Wang, P., Zhang, P., Zhu, Q., Chen, Q., Du, Q., Chen, R. J., Jin, R. L., Ge, R., Pan, R., Xu, R., Chen, R., Li, S. S., Lu, S., Zhou, S., Chen, S., Wu, S., Ye, S., Ma, S., Wang, S., Zhou, S., Yu, S., Zhou, S., Zheng, S., Wang, T., Pei, T., Yuan, T., Sun, T., Xiao, W. L., Zeng, W., An, W., Liu, W., Liang, W., Gao, W., Zhang, W., Li, X. Q., Jin, X., Wang, X., Bi, X., Liu, X., Wang, X., Shen, X., Chen, X., Chen, X., Nie, X., Sun, X., Wang, X., Liu, X., Xie, X., Yu, X., Song, X., Zhou, X., Yang, X., Lu, X., Su, X., Wu, Y., Li, Y. K., Wei, Y. X., Zhu, Y. X., Xu, Y., Huang, Y., Li, Y., Zhao, Y., Sun, Y., Li, Y., Wang, Y., Zheng, Y., Zhang, Y., Xiong, Y., Zhao, Y., He, Y., Tang, Y., Piao, Y., Dong, Y., Tan, Y., Liu, Y., Wang, Y., Guo, Y., Zhu, Y., Wang, Y., Zou, Y., Zha, Y., Ma, Y., Yan, Y., You, Y., Liu, Y., Ren, Z. Z., Ren, Z., Sha, Z., Fu, Z., Huang, Z., Zhang, Z., Xie, Z., Hao, Z., Shao, Z., Wen, Z., Xu, Z., Zhang, Z., Li, Z., Wang, Z., Gu, Z., Li, Z., and Xie, Z. Deepseek-v2: A strong, economical, and efficient mixture-of-experts language model, 2024. URL <https://arxiv.org/abs/2405.04434>.

Dwibedy, D. and Mohanty, R. Online scheduling with makespan minimization: State of the art results, research challenges and open problems, 2020. URL <https://arxiv.org/abs/2001.04698>.

Dwibedy, D. and Mohanty, R. Online list scheduling for makespan minimization: A review of the state-of-the-art results, research challenges and open problems. *SIGACT News*, 53(2):84–105, July 2022. ISSN 0163-5700. doi: 10.1145/3544979.3544993. URL <https://doi.org/10.1145/3544979.3544993>.

Gandhi, S., Zhao, M., Skiadopoulos, A., and Kozyrakis, C. ReCycle: Resilient Training of Large DNNs using Pipeline Adaptation. In *Proceedings of the ACM SIGOPS 30th Symposium on Operating Systems Principles*, SOSP ’24, pp. 211–228, New York, NY, USA, 2024. Association for Computing Machinery. ISBN 9798400712517. doi: 10.1145/3694715.3695960. URL <https://doi.org/10.1145/3694715.3695960>.

Gemini. Gemini 2.5: Our most intelligent AI model. <https://blog.google/technology/google-deepmind/gemini-model-thinking-updates-march-2025/>, 2025.

Github. Github Copilot. <https://github.com/features/copilot/>, 2024.

Google. Tpu architecture. <https://cloud.google.com/tpu/docs/system-architecture-tpu-vm#tpu-pod>.

Guha, E., Marten, R., Keh, S., Raoof, N., Smyrnis, G., Bansal, H., Nezhurina, M., Mercat, J., Vu, T., Sprague, Z., Suvarna, A., Feuer, B., Chen, L., Khan, Z., Frankel, E., Grover, S., Choi, C., Muennighoff, N., Su, S., Zhao, W., Yang, J., Pimpalaonkar, S., Sharma, K., Ji, C. C.-J., Deng, Y., Pratt, S., Ramanujan, V., Saad-Falcon, J., Li, J., Dave, A., Albalak, A., Arora, K., Wulfe, B., Hegde, C., Durrett, G., Oh, S., Bansal, M., Gabriel, S., Grover, A., Chang, K.-W., Shankar, V., Gokaslan, A., Merrill, M. A., Hashimoto, T., Choi, Y., Jitsev, J., Heckel, R., Sathiamoorthy, M., Dimakis, A. G., and Schmidt, L. Openthoughts: Data recipes for reasoning models, 2025. URL <https://arxiv.org/abs/2506.04178>.

He, T., Li, X., Wang, Z., Qian, K., Xu, J., Yu, W., and Zhou, J. Unicron: Economizing self-healing llm training at scale, 2023. URL <https://arxiv.org/abs/2401.00134>.

Hu, Q., Ye, Z., Wang, Z., Wang, G., Zhang, M., Chen, Q., Sun, P., Lin, D., Wang, X., Luo, Y., Wen, Y., and Zhang, T. Characterization of Large Language Model Development in the Datacenter. In *Proceedings of the 21st USENIX Symposium on Networked Systems Design and Implementation*, NSDI’24, USA, 2024. USENIX Association. ISBN 978-1-939133-39-7.

Jang, I., Yang, Z., Zhang, Z., Jin, X., and Chowdhury, M. Oobleck: Resilient Distributed Training of Large Models Using Pipeline Templates. In *Proceedings of the 29th Symposium on Operating Systems Principles*, SOSP '23, pp. 382–395, New York, NY, USA, 2023. Association for Computing Machinery. ISBN 9798400702297. doi: 10.1145/3600006.3613152. URL <https://doi.org/10.1145/3600006.3613152>.

Jeon, M., Venkataraman, S., Qian, J., Phanishayee, A., Xiao, W., and Yang, F. Multi-tenant gpu clusters for deep learning workloads: Analysis and implications. *Technical report, Microsoft Research*, 2018.

Jiang, Z., Lin, H., Zhong, Y., Huang, Q., Chen, Y., Zhang, Z., Peng, Y., Li, X., Xie, C., Nong, S., Jia, Y., He, S., Chen, H., Bai, Z., Hou, Q., Yan, S., Zhou, D., Sheng, Y., Jiang, Z., Xu, H., Wei, H., Zhang, Z., Nie, P., Zou, L., Zhao, S., Xiang, L., Liu, Z., Li, Z., Jia, X., Ye, J., Jin, X., and Liu, X. MegaScale: Scaling Large Language Model Training to More Than 10,000 GPUs. In *21st USENIX Symposium on Networked Systems Design and Implementation (NSDI 24)*, pp. 745–760, Santa Clara, CA, April 2024. USENIX Association. ISBN 978-1-939133-39-7. URL <https://www.usenix.org/conference/nsdi24/presentation/jiang-ziheng>.

Kokolis, A., Kuchnik, M., Hoffman, J., Kumar, A., Malani, P., Ma, F., DeVito, Z., Sengupta, S., Saladi, K., and Wu, C.-J. Revisiting Reliability in Large-Scale Machine Learning Research Clusters. In *2025 IEEE International Symposium on High Performance Computer Architecture (HPCA)*, pp. 1259–1274. IEEE, 2025.

Kwon, W., Li, Z., Zhuang, S., Sheng, Y., Zheng, L., Yu, C. H., Gonzalez, J., Zhang, H., and Stoica, I. Efficient memory management for large language model serving with pagedattention. In *Proceedings of the 29th Symposium on Operating Systems Principles*, SOSP '23, pp. 611–626, New York, NY, USA, 2023. Association for Computing Machinery. ISBN 9798400702297. doi: 10.1145/3600006.3613165. URL <https://doi.org/10.1145/3600006.3613165>.

Maeng, K., Bharuka, S., Gao, I., Jeffrey, M., Saraph, V., Su, B.-Y., Trippel, C., Yang, J., Rabbat, M., Lucia, B., and Wu, C.-J. CPR: Understanding and Improving Failure Tolerant Training for Deep Learning Recommendation with Partial Recovery. *Proceedings of Machine Learning and Systems*, 3:637–651, 2021.

Meta-AI. Introducing meta llama 3: The most capable openly available llm to date. <https://ai.meta.com/blog/meta-llama-3/>, April 2024.

Miao, X., Shi, C., Duan, J., Xi, X., Lin, D., Cui, B., and Jia, Z. Spotserve: Serving generative large language models on preemptible instances. In *Proceedings of the 29th ACM International Conference on Architectural Support for Programming Languages and Operating Systems, Volume 2*, ASPLOS '24, pp. 1112–1127, New York, NY, USA, 2024. Association for Computing Machinery. ISBN 9798400703850. doi: 10.1145/3620665.3640411. URL <https://doi.org/10.1145/3620665.3640411>.

Mistral-AI. Cheaper, better, faster, stronger. <https://mistral.ai/news/mixtral-8x22b>, April 2024.

Mohan, J., Phanishayee, A., and Chidambaram, V. Check-Freq: Frequent, Fine-Grained DNN Checkpointing. In *19th USENIX Conference on File and Storage Technologies (FAST 21)*, pp. 203–216. USENIX Association, February 2021. ISBN 978-1-939133-20-5. URL <https://www.usenix.org/conference/fast21/presentation/mohan>.

NVIDIA. Nvlink and nvlink switch. <https://www.nvidia.com/en-in/data-center/nvlink/>.

NVIDIA. Nvidia gb200 nvl72. <https://www.nvidia.com/en-us/data-center/gb200-nvl72/>, 2025a.

NVIDIA. Dynamo 0.4 delivers 4x faster performance, slo-based autoscaling, and real-time observability. <https://developer.nvidia.com/blog/dynamo-0-4-delivers-4x-faster-performance-slo-based-autoscaling-and-real-time-observability/>, August 2025b.

OpenAI. ChatGPT: Language models for task-oriented dialogue. <https://openai.com/blog/chatgpt/>, 2022.

Ouyang, L., Wu, J., Jiang, X., Almeida, D., Wainwright, C. L., Mishkin, P., Zhang, C., Agarwal, S., Slama, K., Ray, A., Schulman, J., Hilton, J., Kelton, F., Miller, L., Simens, M., Askell, A., Welinder, P., Christiano, P., Leike, J., and Lowe, R. Training language models to follow instructions with human feedback, 2022. URL <https://arxiv.org/abs/2203.02155>.

Qin, R., Li, Z., He, W., Cui, J., Ren, F., Zhang, M., Wu, Y., Zheng, W., and Xu, X. Mooncake: Trading more storage for less computation—a {KVCache-centric} architecture for serving {LLM} chatbot. In *23rd USENIX Conference on File and Storage Technologies (FAST 25)*, pp. 155–170, 2025.

SGLang-Team. Sglang v0.4: Zero-overhead batch scheduler, cache-aware load balancer, faster structured outputs. <https://lmsys.org/blog/2024-12-04-sqlang-v0-4/>, December 2024. LMSYS Blog.

SGLang-Team. Deploying deepseek with pd disaggregation and large-scale expert parallelism on 96 h100 gpus. <https://lmsys.org/blog/2025-05-05-large-scale-ep/>, May 2025. LMSYS Blog.

Shoeybi, M., Patwary, M., Puri, R., LeGresley, P., Casper, J., and Catanzaro, B. Megatron-LM: Training Multi-Billion Parameter Language Models Using Model Parallelism. *CoRR*, abs/1909.08053, 2019. URL <http://arxiv.org/abs/1909.08053>.

Strati, F., McAllister, S., Phanishayee, A., Tarnawski, J., and Klimovic, A. Déjàvu: Kv-cache streaming for fast, fault-tolerant generative llm serving. In *Proceedings of the 41st International Conference on Machine Learning, ICML’24*. JMLR.org, 2024.

Sun, B., Huang, Z., Zhao, H., Xiao, W., Zhang, X., Li, Y., and Lin, W. Llumnix: dynamic scheduling for large language model serving. In *Proceedings of the 18th USENIX Conference on Operating Systems Design and Implementation, OSDI’24*, USA, 2024. USENIX Association. ISBN 978-1-939133-40-3.

Thorpe, J., Zhao, P., Eyolfson, J., Qiao, Y., Jia, Z., Zhang, M., Netravali, R., and Xu, G. H. Bamboo: Making Preemptible Instances Resilient for Affordable Training of Large DNNs. In *20th USENIX Symposium on Networked Systems Design and Implementation (NSDI’23)*, pp. 497–513, Boston, MA, April 2023. USENIX Association. ISBN 978-1-939133-33-5. URL <https://www.usenix.org/conference/nsdi23/presentation/thorpe>.

Vaswani, A., Shazeer, N., Parmar, N., Uszkoreit, J., Jones, L., Gomez, A. N., Kaiser, L., and Polosukhin, I. Attention is all you need. In *Proceedings of the 31st International Conference on Neural Information Processing Systems, NIPS’17*, pp. 6000–6010, Red Hook, NY, USA, 2017. Curran Associates Inc. ISBN 9781510860964.

Wang, Z., Jia, Z., Zheng, S., Zhang, Z., Fu, X., Ng, T. S. E., and Wang, Y. GEMINI: Fast Failure Recovery in Distributed Training with In-Memory Checkpoints. In *Proceedings of the 29th Symposium on Operating Systems Principles, SOSP ’23*, pp. 364–381, New York, NY, USA, 2023. Association for Computing Machinery. ISBN 9798400702297. doi: 10.1145/3600006.3613145. URL <https://doi.org/10.1145/3600006.3613145>.

Wang, Z., Ying, Z., and Zhang, Y. Online makespan minimization: Beat lpt by dynamic locking, 2025. URL <https://arxiv.org/abs/2311.11195>.

Xie, Z., Xu, Z., Zhao, M., An, Y., Mailthody, V. S., Mahlke, S., Garland, M., and Kozyrakis, C. Strata: Hierarchical context caching for long context language model serving. *arXiv preprint arXiv:2508.18572*, 2025.

Yu, G.-I., Jeong, J. S., Kim, G.-W., Kim, S., and Chun, B.-G. Orca: A distributed serving system for Transformer-Based generative models. In *16th USENIX Symposium on Operating Systems Design and Implementation (OSDI’22)*, pp. 521–538, Carlsbad, CA, July 2022. USENIX Association. ISBN 978-1-939133-28-1. URL <https://www.usenix.org/conference/osdi22/presentation/yu>.

Zeng, S., Xie, M., Gao, S., Chen, Y., and Lu, Y. Medusa: Accelerating serverless llm inference with materialization. In *Proceedings of the 30th ACM International Conference on Architectural Support for Programming Languages and Operating Systems, Volume 1, ASPLOS ’25*, pp. 653–668, New York, NY, USA, 2025. Association for Computing Machinery. ISBN 9798400706981. doi: 10.1145/3669940.3707285. URL <https://doi.org/10.1145/3669940.3707285>.

Zheng, L., Yin, L., Xie, Z., Sun, C., Huang, J., Yu, C. H., Cao, S., Kozyrakis, C., Stoica, I., Gonzalez, J. E., Barrett, C., and Sheng, Y. Sqlang: efficient execution of structured language model programs. In *Proceedings of the 38th International Conference on Neural Information Processing Systems, NIPS’24*, Red Hook, NY, USA, 2025. Curran Associates Inc. ISBN 9798331314385.

Zhong, Y., Liu, S., Chen, J., Hu, J., Zhu, Y., Liu, X., Jin, X., and Zhang, H. DistServe: Disaggregating prefill and decoding for goodput-optimized large language model serving. In *18th USENIX Symposium on Operating Systems Design and Implementation (OSDI’24)*, pp. 193–210, Santa Clara, CA, July 2024. USENIX Association. ISBN 978-1-939133-40-3. URL <https://www.usenix.org/conference/osdi24/presentation/zhong-yinmin>.

Zu, Y., Ghaffarkhah, A., Dang, H.-V., Towles, B., Hand, S., Huda, S., Bello, A., Kolbasov, A., Rezaei, A., Du, D., Lacy, S., Wang, H., Wisner, A., Lewis, C., and Bahini, H. Resiliency at Scale: Managing Google’s TPUv4 Machine Learning Supercomputer. In *21st USENIX Symposium on Networked Systems Design and Implementation (NSDI’24)*, pp. 761–774, Santa Clara, CA, April 2024. USENIX Association. ISBN 978-1-939133-39-7. URL <https://www.usenix.org/conference/nsdi24/presentation/zu>.